

Low-energy η -nucleon interaction studied with η photoproduction off the deuteron

S. X. Nakamura,¹ H. Kamano,^{2,3} and T. Ishikawa⁴

¹*Department of Physics, Osaka University, Toyonaka, Osaka 560-0043, Japan*

²*KEK Theory Center, Institute of Particle and Nuclear Studies (IPNS),*

High Energy Accelerator Research Organization (KEK), Tsukuba, Ibaraki 305-0801, Japan

³*J-PARC Branch, KEK Theory Center, IPNS, KEK, Tokai, Ibaraki 319-1106, Japan*

⁴*Research Center for Electron Photon Science (ELPH),
Tohoku University, Sendai, Miyagi 982-0826, Japan*

We develop a reaction model for η photoproduction off the deuteron ($\gamma d \rightarrow \eta pn$), and study the reaction at a special kinematics, where the photon beam energy is ~ 0.94 GeV and the scattered proton is detected at $\sim 0^\circ$, for the purpose of determining the η -nucleon scattering length ($a_{\eta N}$) and effective range ($r_{\eta N}$). In this kinematics, the η -nucleon elastic rescattering is significantly enhanced while other background mechanisms being suppressed. We show that a ratio R , the $\gamma d \rightarrow \eta pn$ cross section divided by the $\gamma p \rightarrow \eta p$ cross section convoluted with the proton momentum distribution in the deuteron, has a very good resolving power of $a_{\eta N}$ and $r_{\eta N}$. We conclude that the R data with 5% error, binned in 1 MeV width of the η -neutron invariant mass, can determine $\text{Re}[a_{\eta N}]$ ($\text{Re}[r_{\eta N}]$) at the precision of $\sim \pm 0.1$ fm ($\sim \pm 0.5$ fm), significantly narrowing down the previously estimated ranges of the parameters. To arrive at the conclusion, it is essential to use the $\gamma d \rightarrow \eta pn$ reaction model equipped with elementary amplitudes that are well constrained by πN and γN reaction data through a sophisticated coupled-channels analysis. This result strongly motivates the ELPH facility at Tohoku University to measure R .

The low-energy interaction between the η meson and the nucleon (N) is, as with the πN interaction, a basic feature of the meson-baryon dynamics. It is characterized by the two complex parameters, the scattering length $a_{\eta N}$ and effective range $r_{\eta N}$, defined through an effective-range expansion of the S -wave ηN scattering amplitude: $F_{\eta N}(k) = [k \cot \delta(k) - ik]^{-1}$ with $k \cot \delta(k) = a_{\eta N}^{-1} + (1/2)r_{\eta N}k^2 + O(k^4)$, where k is the on-shell η momentum in the center-of-mass (CM) frame and $\delta(k)$ the phase shift. Because $a_{\eta N}$ determines the attractive or repulsive nature of the ηN interaction at $k \sim 0$, the existence of exotic η -mesic nuclei, which have been actively searched for experimentally, hinges on its value (see, e.g., Refs. [1, 2]). Accurate values of $a_{\eta N}$ and $r_{\eta N}$ can also greatly help determine the pole position of the S -wave $N(1535)1/2^-$ resonance, the first spin-1/2 negative-parity excitation of the nucleon; the pole is known to be near the ηN threshold but its accurate position is still uncertain [3]. It is known that the S -wave scattering parameters can well determine an S -wave resonance pole near threshold (see, e.g., Refs. [4, 5]).

Despite its important role in nuclear and hadron physics, the low-energy ηN interaction has not been well understood yet. This is attributed mainly to the fact that neither direct ηN scattering experiments nor X -ray measurements from η -mesic atoms are possible due to the neutral and unstable nature of η , and thus one has to rely on indirect information. Previous works have attempted to extract $a_{\eta N}$ and $r_{\eta N}$ by analyzing the $\pi N \rightarrow \pi N, \eta N$ and $\gamma N \rightarrow \pi N, \eta N$ reaction data that have a sensitivity to the ηN interaction through coupled-channels effects [2]. The $pn \rightarrow \eta d$ reaction has also been analyzed to extract the ηN interaction embedded in the strongly interacting ηNN system [6, 7]. These analyses gave fairly

convergent results for the imaginary parts of $a_{\eta N}$ and $r_{\eta N}$, the values of which fall into $\text{Im}[a_{\eta N}] = 0.2 - 0.3$ fm and $\text{Im}[r_{\eta N}] = -1 - 0$ fm, respectively, as compiled in Refs. [2, 8]. However, their real parts scatter in a rather wide range: $\text{Re}[a_{\eta N}] = 0.2 - 0.9$ fm and $\text{Re}[r_{\eta N}] = -6 - +1$ fm. The wide range of the previously extracted $\text{Re}[a_{\eta N}]$ and $\text{Re}[r_{\eta N}]$ originates from the difficulty of isolating the ηN scattering amplitudes from other mechanisms involved in the reactions analyzed. Therefore, it is highly desirable to utilize reactions in which mechanisms associated with the ηN elastic rescattering are significantly enhanced while other background mechanisms being suppressed.

To meet this demand, an η photoproduction experiment [9] is planned at the Research Center for Electron Photon Science (ELPH), Tohoku University. In this experiment, a deuteron target is irradiated with a photon beam at the laboratory (Lab) energy of $E_\gamma \sim 0.94$ GeV [10, 11], and the scattered proton from the $\gamma d \rightarrow \eta pn$ reaction is detected at $\theta_p \sim 0^\circ$ from the photon direction. At this chosen kinematics, an η is likely to be produced almost at rest, being expected to strongly interact with the spectator neutron. Meanwhile, the struck proton goes away with a large momentum, leaving little chance to interact with the η and neutron. This seems an ideal kinematical condition, to which we refer as the ELPH kinematics, to determine the low-energy ηN scattering parameters. In this work, we show with a theoretical analysis that a combined cross-section data for $\gamma d \rightarrow \eta pn$ and $\gamma p \rightarrow \eta p$ expected to be taken at the ELPH experiment would indeed lead to significant reduction of the uncertainty of $a_{\eta N}$ and $r_{\eta N}$ previously extracted, thereby providing crucial constraints on the existence of η -mesic nuclei and the properties of

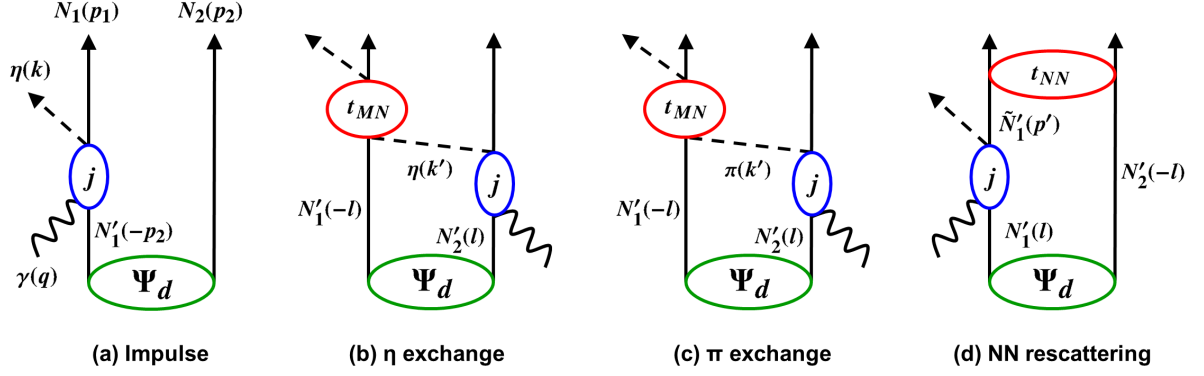


FIG. 1. Diagrammatic representation of reaction mechanisms considered in this work for $\gamma d \rightarrow \eta N_1 N_2$: (a) impulse, (b) η -exchange, (c) π -exchange, and (d) NN rescattering mechanisms. Labels for particles along with their momenta in the Lab frame are indicated. The external lines are the same for all the diagrams and thus their labels are indicated in (a) only. Also, $\mathbf{k}' = \mathbf{q} - \mathbf{p}_2 + \mathbf{l}$ and $\mathbf{p}' = \mathbf{q} - \mathbf{k} + \mathbf{l}$.

$N(1535)1/2^-$.

Reaction mechanisms for $\gamma d \rightarrow \eta pn$ relevant to the ELPH experiment are depicted in Fig. 1. Here, the η -exchange mechanism [Fig. 1(b)] contains the $\eta N \rightarrow \eta N$ subprocess we are interested in, while the other mechanisms (the impulse [Fig. 1(a)], π -exchange [Fig. 1(c)],

and NN -rescattering [Fig. 1(d)] mechanisms) are backgrounds for our purpose. With the definition of the momenta shown in Fig. 1, the amplitudes corresponding to each of the mechanisms, T_{imp} (impulse), T_η (η -exchange), T_π (π -exchange), and T_N (NN -rescattering), are explicitly written in the Lab frame as

$$T_{\text{imp}} = \sqrt{2} \sum_{s'_1} \langle \eta(\mathbf{k}) N_1(\mathbf{p}_1, s_1, t_1) | j(M_{\eta N_1}) | \gamma(\mathbf{q}, \mu) N'_1(-\mathbf{p}_2, s'_1, t_1) \rangle \langle N'_1(-\mathbf{p}_2, s'_1, t_1) N_2(\mathbf{p}_2, s_2, t_2) | \Psi_d(s_d) \rangle, \quad (1)$$

$$T_{M(=\eta, \pi^\pm, \pi^0)} = \sqrt{2} \sum_{s'_1, s'_2, t'_1, t'_2} \int d\mathbf{l} \langle \eta(\mathbf{k}) N_1(\mathbf{p}_1, s_1, t_1) | t_{MN}(M_{\eta N_1}) | M(\mathbf{q} - \mathbf{p}_2 + \mathbf{l}) N'_1(-\mathbf{l}, s'_1, t'_1) \rangle \\ \times \frac{\langle M(\mathbf{q} - \mathbf{p}_2 + \mathbf{l}) N_2(\mathbf{p}_2, s_2, t_2) | j(W) | \gamma(\mathbf{q}, \mu) N'_2(\mathbf{l}, s'_2, t'_2) \rangle}{E - E_N(\mathbf{p}_2) - E_N(-\mathbf{l}) - E_M(\mathbf{q} - \mathbf{p}_2 + \mathbf{l}) + i\epsilon} \langle N'_1(-\mathbf{l}, s'_1, t'_1) N'_2(\mathbf{l}, s'_2, t'_2) | \Psi_d(s_d) \rangle, \quad (2)$$

$$T_N = \sqrt{2} \sum_{s'_1, \tilde{s}'_1, s'_2} \int d\mathbf{l} \langle N_1(\mathbf{p}_1, s_1, t_1) N_2(\mathbf{p}_2, s_2, t_2) | t_{NN}(M_{N_1 N_2}) | \tilde{N}'_1(\mathbf{q} - \mathbf{k} + \mathbf{l}, \tilde{s}'_1, t_1) N'_2(-\mathbf{l}, s'_2, t_2) \rangle \\ \times \frac{\langle \eta(\mathbf{k}) \tilde{N}'_1(\mathbf{q} - \mathbf{k} + \mathbf{l}, \tilde{s}'_1, t_1) | j(W) | \gamma(\mathbf{q}, \mu) N'_1(\mathbf{l}, s'_1, t_1) \rangle}{E - E_N(\mathbf{q} - \mathbf{k} + \mathbf{l}) - E_N(-\mathbf{l}) - E_\eta(\mathbf{k}) + i\epsilon} \langle N'_1(\mathbf{l}, s'_1, t_1) N'_2(-\mathbf{l}, s'_2, t_2) | \Psi_d(s_d) \rangle, \quad (3)$$

plus the exchange terms obtained from Eqs. (1)–(3) by flipping the overall sign and interchanging all subscripts 1 and 2 such as $\{N_1^{(i)}, \mathbf{p}_1, s_1^{(i)}, t_1^{(i)}\} \leftrightarrow \{N_2^{(i)}, \mathbf{p}_2, s_2^{(i)}, t_2^{(i)}\}$. Here, $|\Psi_d(s_d)\rangle$ is the deuteron state at rest with spin projection s_d ; $|N(\mathbf{p}, s, t)\rangle$ the nucleon state with momentum \mathbf{p} and spin and isospin projections s and t ; $|\gamma(\mathbf{q}, \mu)\rangle$ the photon state with momentum \mathbf{q} and polarization μ ; and $|M(\mathbf{k})\rangle$ ($M = \eta, \pi^\pm, \pi^0$) the pseudoscalar meson state with momentum \mathbf{k} . The total scattering energy E of the system in the Lab frame is given by the sum

of the photon Lab energy and the deuteron rest mass, $E = E_\gamma + m_d$, and the invariant masses of the two-body subprocesses in the above equations are defined to be $M_{\eta N_1} = \{[E_\eta(\mathbf{k}) + E_N(\mathbf{p}_1)]^2 - (\mathbf{k} + \mathbf{p}_1)^2\}^{1/2}$, $W = \{[E - E_N(-\mathbf{l})]^2 - (\mathbf{l} + \mathbf{q})^2\}^{1/2}$, and $M_{N_1 N_2} = \{[E_N(\mathbf{p}_1) + E_N(\mathbf{p}_2)]^2 - (\mathbf{p}_1 + \mathbf{p}_2)^2\}^{1/2}$, where $E_x(\mathbf{p}) = \sqrt{m_x^2 + \mathbf{p}^2}$ with m_x being the mass of a particle x . The elementary (half-off-shell) amplitudes for photoproduction, meson-baryon, and NN rescattering

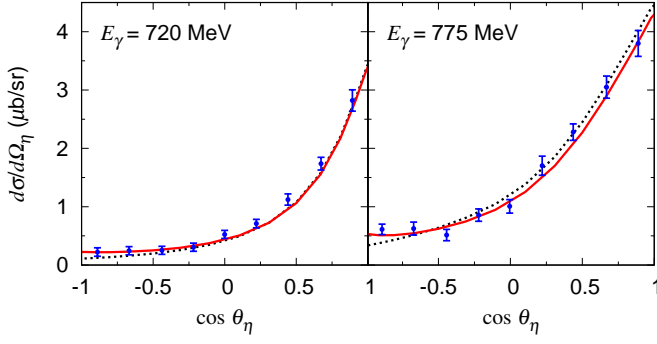


FIG. 2. Angular distributions of η in $\gamma d \rightarrow \eta pn$ in the γd CM frame. The photon Lab energy (E_γ) is indicated in each panel. The solid curves are from the full calculation, while the dotted curves are obtained with the impulse mechanism only. The data are for the semi-inclusive $\gamma d \rightarrow \eta X$ process [16]; the coherent contribution is negligible here [17].

are denoted by $\langle MN|j|\gamma N'\rangle$, $\langle MN|t_{MN}|M'N'\rangle$, and $\langle N_1 N_2|t_{NN}|N'_1 N'_2\rangle$, respectively.

Our task is to develop a $\gamma d \rightarrow \eta pn$ reaction model to evaluate Eqs. (1)–(3) and reliably isolate the amplitude for the $\eta N \rightarrow \eta N$ subprocess from data with well-predicted contributions from all the other background mechanisms. Such a model must be built with reliable amplitudes for elementary $\gamma N \rightarrow MN$, $MN \rightarrow M'N$, and $NN \rightarrow NN$ processes with $M^{(\prime)} = \pi, \eta$, as well as with a realistic deuteron wave function. Regarding $\gamma N \rightarrow MN$ and $MN \rightarrow M'N$ amplitudes, we employ those generated with a dynamical coupled-channels (DCC) model [12, 13]. The DCC model is a multichannel unitary model for the πN and γN reactions in the nucleon resonance region. It was constructed fitting $\sim 27,000$ data points, and successfully describes [12–14] $\pi N \rightarrow \pi N, \pi\pi N, \eta N, K\Lambda, K\Sigma$ and $\gamma N \rightarrow \pi N, \pi\pi N, \eta N, K\Lambda, K\Sigma$ reactions over the energy region from the thresholds up to $\sqrt{s} \lesssim 2.1$ GeV. This DCC model predicts the ηN scattering parameters to be $a_{\eta N} = 0.75 + 0.26i$ fm and $r_{\eta N} = -1.6 - 0.6i$ fm, which are consistent with the previously estimated ranges. As for the deuteron wave function and the NN scattering amplitudes, we employ those generated with the CD-Bonn potential [15].

The setup described above allows us to make a parameter-free prediction for the $\gamma d \rightarrow \eta pn$ cross sections. We thus confront our model predictions with existing data, thereby assessing the validity of the model. In Fig. 2, we show the η angular distribution at $E_\gamma = 720$ and 775 MeV from our DCC-based model with and without the rescattering contributions along with the data. Our parameter-free prediction is found to be in an excellent agreement with the data. A slight enhancement in the backward direction due to the $\eta N \rightarrow \eta N$ rescattering is important for this agreement. Fix *et al.* [18] also have done a comparable calculation, and found a rather mi-

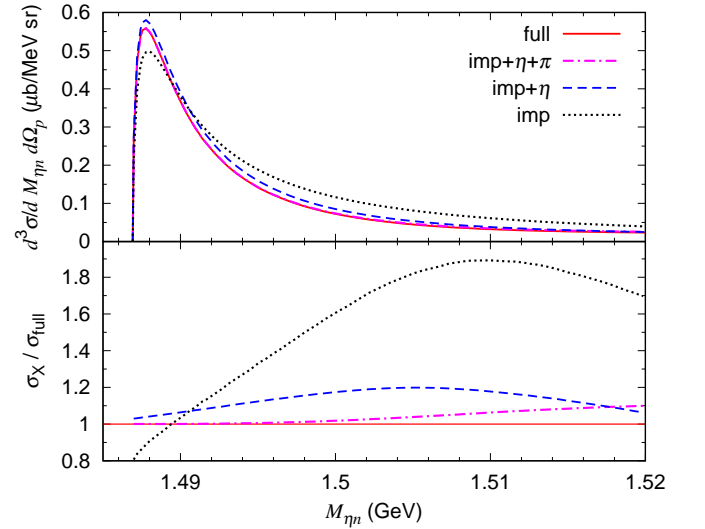


FIG. 3. (Top) Threefold differential cross section, $d^3\sigma/dM_\eta d\Omega_p$, for $\gamma d \rightarrow \eta pn$ at $E_\gamma = 0.94$ GeV and $\theta_p = 0^\circ$, plotted as a function of M_η . The results are from the full calculation (solid curve), the impulse mechanism only (dotted curve), the impulse and η -exchange mechanisms (dashed curve), and the impulse, η - and π -exchange mechanisms (dash-dotted curve). The dash-dotted curve falls almost exactly on the solid curve. (Bottom) Ratios of the differential cross sections calculated with the various mechanisms to those from the full calculation.

nor role of the $\eta N \rightarrow \eta N$ rescattering mechanism in the η angular distribution at these energies. The slight underestimation of their results at backward angles (Fig. 5 of Ref. [18]) is likely to be ascribable to the different ηN scattering lengths; $a_{\eta N} = 0.75 + 0.26i$ fm in our model and $a_{\eta N} = 0.5 + 0.32i$ fm in Ref. [18].

Now let us consider the $\gamma d \rightarrow \eta pn$ reaction at the ELPH kinematics with $E_\gamma = 0.94$ GeV and $\theta_p = 0^\circ$. In Fig. 3(top), our model predictions for the threefold differential cross section, $d^3\sigma/dM_\eta d\Omega_p$, are presented as a function of M_η . We find that the dominant contribution is from the impulse mechanism [Fig. 1(a)] that contains the $\gamma p \rightarrow \eta p$ amplitudes, while the $\gamma n \rightarrow \eta n$ amplitudes negligibly contributes. The η -exchange mechanism [Fig. 1(b)] has a substantial contribution to the cross section, which changes the impulse result by $-60 - +20\%$ [difference between the dashed and dotted curves in Fig. 3(bottom)]. Meanwhile, the π -exchange [Fig. 1(c)] contribution is smaller, and suppresses the cross sections by $\lesssim 15\%$ (difference between the dashed and dash-dotted curves). The NN rescattering [Fig. 1(d)] contribution [deviation of the dash-dotted curve from 1 in Fig. 3(bottom)] is very small for $M_\eta \lesssim 1.5$ GeV. This feature is what we expect to find in this special kinematics. The suppression of the π -exchange mechanism can be attributed to the fact that the exchanged pions have rather large momenta near their on-shell, picking

up high-momentum components with very small probabilities in the deuteron wave function. Our numerical analysis with the well-controlled elementary amplitudes demonstrates that this kinematical suppression is strong enough to lead to a rather small contribution of the π -exchange mechanism, even though the elementary $\gamma p \rightarrow \pi N$ amplitude is significantly larger than that of $\gamma p \rightarrow \eta p$ at the considered energies. The NN -rescattering mechanism is hindered by the same kinematical reason, and also by the rather weak NN scattering at this kinematics where the NN relative momentum is large.

We have shown that the $\gamma d \rightarrow \eta pn$ in the ELPH kinematics for $M_{\eta n} \lesssim 1.5$ GeV are mostly described with the impulse and η -exchange mechanisms and with the smaller (almost negligible) correction from the π -exchange (NN -rescattering) mechanism. This indicates that the proton is well separated from interacting with the ηn system, and thus multiple rescatterings beyond the first-order rescattering [Fig. 1(b)-(d)] should be safely neglected in this kinematical region. We have also confirmed that an off-shell momentum effect associated with the $\eta n \rightarrow \eta n$ scattering amplitude is very small and that ηn partial waves higher than the S wave give negligibly small contributions. These facts allow us to modify the full $\gamma d \rightarrow \eta pn$ model by replacing the ηn scattering amplitude with the S -wave one parametrized with $a_{\eta N}$ and $r_{\eta N}$, and then to determine these parameters through analyzing the forthcoming ELPH data. To make contact with the ELPH data, we need to take one more step because the data are actually given in a form of the ratio, denoted by R_{exp} , of the measured cross sections for $\gamma d \rightarrow \eta pn$ divided by those for $\gamma p \rightarrow \eta p$ convoluted with the proton momentum distribution in the deuteron. This is for removing systematic uncertainties of the acceptance from the detector coverage. Thus, from the theoretical side, the corresponding quantity to calculate is:

$$R_{\text{th}}(M_{\eta n}) = \frac{d^3\sigma_{\text{full}}/dM_{\eta n}d\Omega_p|_{\theta_p=0^\circ}}{d^3\sigma_{\text{imp}}/dM_{\eta n}d\Omega_p|_{\theta_p=0^\circ}}, \quad (4)$$

where σ_{full} (σ_{imp}) is calculated with the modified full model (the impulse term only). The remaining questions to address are how sensitively R_{th} changes as $a_{\eta N}$ and $r_{\eta N}$ are varied, and how well R_{exp} with a certain error can determine $a_{\eta N}$ and $r_{\eta N}$.

First we vary $\text{Re}[a_{\eta N}]$ over 0.2 – 1.0 fm, with fixed values of $\text{Im}[a_{\eta N}] = 0.25$ fm and $r_{\eta N} = 0$ fm. At the ELPH kinematics and $M_{\eta n} \leq 1.505$ GeV, the obtained cross sections are mostly within the red striped region shown in Fig. 4(top). The corresponding variation of R_{th} is shown in Fig. 4(bottom) where the sensitivity to the variation of $\text{Re}[a_{\eta N}]$ is more clearly seen. As the striped bands show, the cross section and thus R_{th} changes by $\sim 24\%$ at the quasi-free (QF) peak position at $M_{\eta n} \sim 1.488$ GeV. Meanwhile, the green solid bands, which are covered when $\text{Re}[a_{\eta N}]$ is varied by ± 0.1 fm

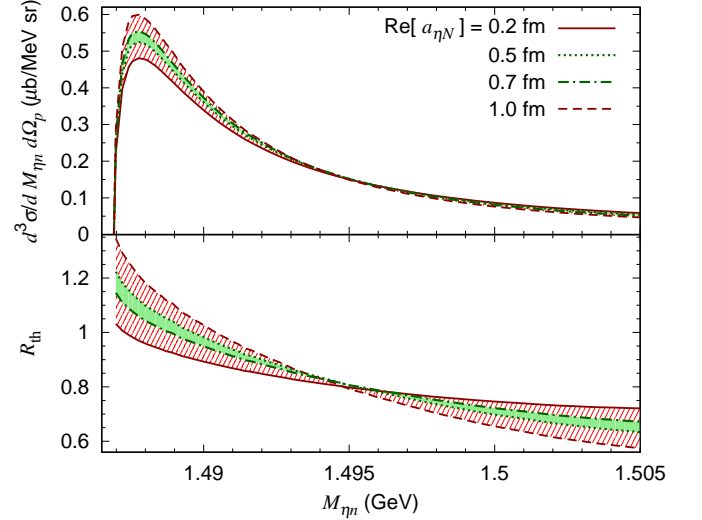


FIG. 4. (Top) $\text{Re}[a_{\eta N}]$ -dependence of $\gamma d \rightarrow \eta pn$ differential cross sections at $E_\gamma = 0.94$ GeV and $\theta_p = 0^\circ$ calculated with the full model. The solid, dotted, dash-dotted, and dashed curves are obtained with $\text{Re}[a_{\eta N}] = 0.2, 0.5, 0.7$, and 1.0 fm, respectively; $\text{Im}[a_{\eta N}] = 0.25$ fm and $r_{\eta N} = 0$. (Bottom) The quantity R_{th} defined in Eq. (4) for various values of $\text{Re}[a_{\eta N}]$.

from 0.6 fm, have the widths of $\sim 5\%$ at the QF peak. The result indicates that R_{exp} data of 5% error per MeV bin, which is achievable in the planned ELPH experiment [9], can determine $\text{Re}[a_{\eta N}]$ at the precision of $\sim \pm 0.1$ fm, significantly narrowing down the current uncertainty.

Next we vary $\text{Re}[r_{\eta N}]$ over a rather broad range of the current estimates, $-6 - 0$ fm; the scattering length is fixed at $a_{\eta n} = 0.75 + 0.26i$ fm, the value from the latest DCC analysis [13]; $\text{Im}[r_{\eta N}] = 0$ fm. The corresponding changes of the cross section and R_{th} cover the red striped region in Fig. 5. Because $r_{\eta N}$ plays no role very close to the ηN threshold, its effect starts to be visible at ~ 5 MeV above the threshold. The red striped (green solid) band of R_{th} shows that R_{th} at $M_{\eta n} = 1.5$ GeV changes by $\sim 30\%$ ($\sim 6\%$) when $\text{Re}[r_{\eta N}]$ is varied over $-6 - 0$ fm ($-3.5 - -2.5$ fm). Therefore, R_{exp} data of 5% error per MeV bin can also determine $\text{Re}[r_{\eta N}]$ at the precision of $\lesssim \pm 0.5$ fm, significantly improved precision than the current estimates.

Regarding the imaginary part, we vary $\text{Im}[a_{\eta N}]$ in the range of 0.2 – 0.3 fm, the currently estimated range, and with $\text{Re}[a_{\eta N}] = 0.6$ fm and $r_{\eta N} = 0$ fm. The cross sections and R_{th} change at most 5%. When varying $\text{Im}[r_{\eta N}]$ over the currently estimated range, $-1 - 0$ fm, with $a_{\eta n} = 0.75 + 0.26i$ fm and $\text{Re}[r_{\eta N}] = 0$ fm being fixed, we found a similar situation.

Finally, we argue that theoretical uncertainty hardly affect the above results. Here, we stress that it is not the cross section itself but R_{th} that is needed to analyze the ELPH data. A great advantage of using R_{th} is that a large portion of theoretical uncertainty in the

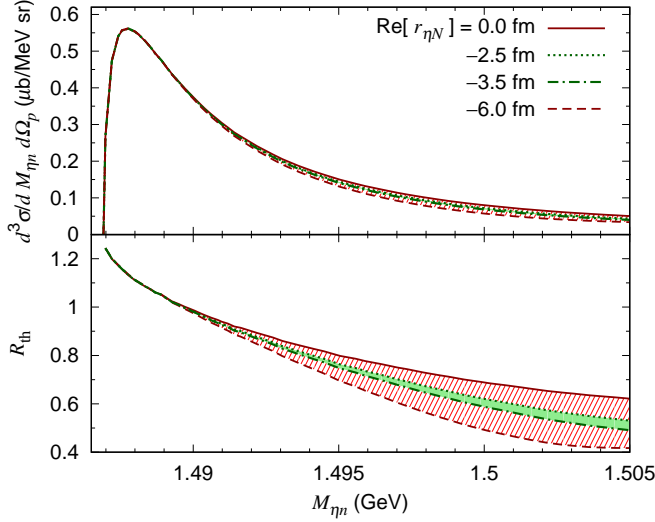


FIG. 5. Similar presentation to Fig. 4, but using $\text{Re}[r_{\eta N}] = 0$ fm (solid), -2.5 fm (dotted), -3.5 fm (dash-dotted), and -6 fm (dashed); $a_{\eta n} = 0.75 + 0.26i$ fm and $\text{Im}[r_{\eta n}] = 0$ fm are fixed.

cross section is cancelled out. For example, a major part of the uncertainty of the cross section is from the elementary $\gamma p \rightarrow \eta p$ amplitudes that carry over errors ($\sim \pm 5\%$) of the cross section data fitted. However, we have confirmed that R_{th} is very stable ($\lesssim 0.1\%$) even when the overall magnitude of the $\gamma p \rightarrow \eta p$ amplitudes is varied over $\pm 3\%$. Another possible source of the uncertainty is the model dependence of the deuteron wave function. We used those of the CD-Bonn [15], Nijmegen I [19], and Reid93 [19] models, and found a rather good stability ($< 0.5\%$ at the QF peak; $\lesssim 1\%$ at $M_{\eta n} \sim 1.5$ GeV) of R_{th} .

In conclusion, we have analyzed the $\gamma d \rightarrow \eta p n$ reaction at $E_\gamma = 0.94$ GeV and $\theta_p = 0^\circ$, and found that, once R_{exp} data of 5% error binned in 1 MeV width are given, $\text{Re}[a_{\eta N}]$ ($\text{Re}[r_{\eta N}]$) can be determined at the precision of $\sim \pm 0.1$ fm ($\sim \pm 0.5$ fm), which is significantly better than

the currently estimated uncertainty. We emphasize that, for reliably extracting the ηN scattering parameters from the data, it is prerequisite to control all the relevant subprocess in $\gamma d \rightarrow \eta p n$ with a sophisticated model like the DCC model [12, 13].

This work was supported by JSPS KAKENHI Grant Numbers JP25105010, JP25800149, and JP26400287.

-
- [1] Q. Haider and L. C. Liu, Phys. Lett. B **172**, 257 (1986).
 - [2] Q. Haider and L. C. Liu, Int. J. Mod. Phys. E **24**, 1530009 (2015).
 - [3] C. Patrignani *et al.* (Particle Data Group), Chin. Phys. C **40**, 100001 (2016).
 - [4] Y. Ikeda, T. Hyodo, D. Jido, H. Kamano, T. Sato, and K. Yazaki, Prog. Theor. Phys. **125**, 1205 (2011).
 - [5] H. Kamano, S. X. Nakamura, T.-S. H. Lee, and T. Sato, Phys. Rev. C **92**, 025205 (2015).
 - [6] H. Garcilazo and M. T. Peña, Eur. Phys. J. A **38**, 209 (2008).
 - [7] H. Calén *et al.*, Phys. Rev. Lett. **79**, 2642 (1997); H. Calén *et al.*, Phys. Rev. Lett. **80**, 2069 (1998).
 - [8] A. M. Green and S. Wycech, Phys. Rev. C **71**, 014001 (2005); Erratum: Phys. Rev. C **72**, 029902 (2005).
 - [9] T. Ishikawa *et al.*, ELPH-2844 experiment (2016); T. Ishikawa *et al.*, JPS Conf. Proc. **13**, 020031 (2017); T. Ishikawa *et al.*, Nucl. Instrum. Meth. A **832**, 108 (2016).
 - [10] T. Ishikawa *et al.*, Nucl. Instrum. Meth. A **622**, 1 (2010).
 - [11] T. Ishikawa *et al.*, Nucl. Instrum. Meth. A **811**, 124 (2016).
 - [12] H. Kamano, S. X. Nakamura, T.-S. H. Lee, and T. Sato, Phys. Rev. C **88**, 035209 (2013).
 - [13] H. Kamano, S. X. Nakamura, T.-S. H. Lee, and T. Sato, Phys. Rev. C **94**, 015201 (2016).
 - [14] H. Kamano, Phys. Rev. C **88**, 045203 (2013).
 - [15] R. Machleidt, Phys. Rev. C **63**, 024001 (2001).
 - [16] B. Krusche *et al.*, Phys. Lett. B **358**, 40 (1995).
 - [17] J. Weiß *et al.*, Eur. Phys. J. A **11**, 371 (2001).
 - [18] A. Fix, H. Arenhövel, M. Levchuk, and M. Tammam, Phys. Rev. C **91**, 014001 (2015).
 - [19] V. G. J. Stoks, R. A. M. Klomp, C. P. F. Terheggen, and J. J. de Swart, Phys. Rev. C **49**, 2950 (1994).